ACS Medicinal Chemistry Letters

Letter

pubs.acs.org/acsmedchemlett

Pyrimidine-Based Tricyclic Molecules as Potent and Orally Efficacious Inhibitors of Wee1 Kinase

Yunsong Tong,*[,†] Maricel Torrent,[‡] Alan S. Florjancic,[†] Kenneth D. Bromberg,[†] Fritz G. Buchanan,[†] Debra C. Ferguson,[†] Eric F. Johnson,[†] Loren M. Lasko,[†] David Maag,[†] Philip J. Merta,[∥] Amanda M. Olson,[§] Donald J. Osterling,[§] Nirupama Soni,[†] Alexander R. Shoemaker,[†] and Thomas D. Penning[†]

[†]Cancer Research, [‡]Molecular Modeling, [§]Pharmacology, and [∥]High Throughput Biology, Research and Development, AbbVie, 1 North Waukegan Road, North Chicago, Illinois 60064-6114, United States

Supporting Information

ABSTRACT: Aided by molecular modeling, compounds with a pyrimidine-based tricyclic scaffold were designed and confirmed to inhibit Wee1 kinase. Structure−activity studies identified key pharmacophores at the aminoaryl and halobenzene regions responsible for binding affinity with sub-nM K_i values. The potent inhibitors demonstrated sub-μM activities in both functional and mechanism-based cellular assays and also possessed desirable pharmacokinetic profiles. The lead molecule, **31**, showed oral efficacy in potentiating the antiproliferative activity of irinotecan, a cytotoxic agent, in a NCI-H1299 mouse xenograft model.

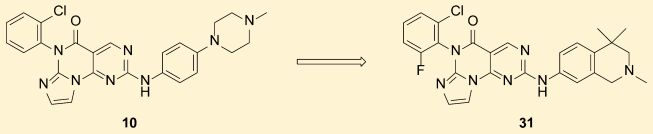

KEYWORDS: *Wee1 kinase inhibitors, antitumor*

Cells utilize G1 and G2/M checkpoints within cell cycle to ensure genomic integrity. The fact that cancer cells are often defective in the G1 checkpoint due to frequent p53 mutations has led to interest in developing anticancer agents that abrogate G2/M arrest.[1,2] One of the key players in this arena is the Wee1 kinase, an atypical tyrosine kinase that phosphorylates Cdk1 (also called Cdc2) on tyrosine 15 (Y15) resulting in functional inactivation.[3] Cdk1 recruits Cyclin A and Cyclin B to initiate mitosis. Wee1 negatively regulates Cdk1 and enables repair of damaged DNA in G2 phase prior to mitosis. Therefore, inhibition of Wee1 forces tumor cells into premature mitosis, leading to mitotic catastrophe and cell death.[4,5] Since Wee1 is overexpressed in certain malignancies,[6−8] Wee1 inhibitors have the potential to sensitize p53 deficient tumors to DNA-damaging treatments.

Recently, a few classes of Wee1 inhibitors have been disclosed.[9−11] Among them is a selective inhibitor, MK-1775 (**1**, 2-allyl-1-(6-(2-hydroxypropan-2-yl)pyridin-2-yl)-6-((4-(4-methylpiperazin-1-yl)phenyl)amino)-1*H*-pyrazolo[3,4-*d*]-pyrimidin-3(2*H*)-one).[9] MK-1775 exhibited antitumor activity in various preclinical studies in potentiating chemo- and radiotherapy and is currently in phase I/II human clinical trials.[12] In addition, a different class of Wee1 inhibitors featuring an imino-dihydropyrimidinone pyrimidine core (**2**) has emerged in patent literature.[13] Computer-assisted evaluation of the Wee1 kinase binding site, using public X-ray structures of bound Wee1 inhibitors as starting points,[14,15] revealed a key region within the ATP binding pocket in Wee1 adjacent to the bicyclic core not utilized by inhibitors such as **2**. This region is generally occupied by the pyridyl moiety of MK-1775 (**1**) and was deemed to be accessible from the ligand hinge region and therefore exploitable for drug design purposes. Taking advantage of this untapped region by **2**, our *de novo* design and modeling studies suggested that molecules with a tricyclic core, as displayed in **3**, would possess key elements for interacting with the active site of the Wee1 protein (see Figure 1A for more details), potentially resulting in improved Wee1 inhibition. In this letter, we demonstrate that not only do such molecules show potent activity in enzymatic and cellular assays but they also exhibit desirable pharmacokinetic properties as well as oral antitumor efficacy in a murine xenograft model.

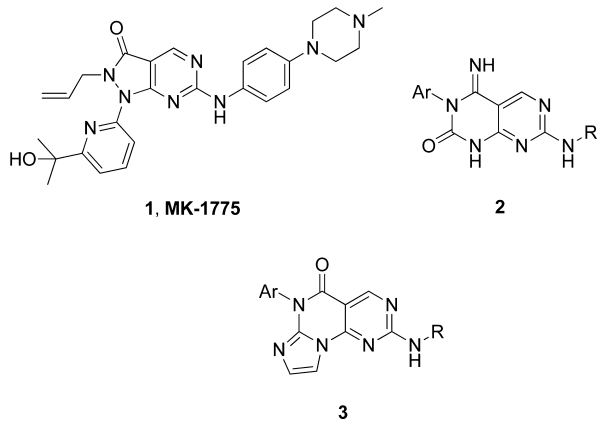

Special Issue: New Frontiers in Kinases

Received: July 2, 2014
Accepted: August 4, 2014
Published: August 6, 2014

The general synthesis of analogs presented in this letter is outlined in Scheme 1. The known amino pyrimidine **4** was

Scheme 1[a]

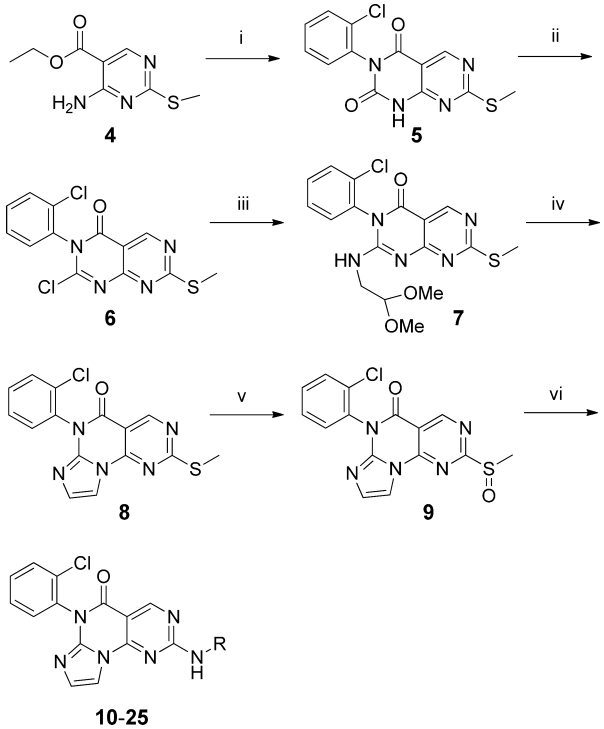

[a]Reagents and conditions: (i) NaH, 1-Cl-2-isocyanatobenzene, 98%; (ii) $POCl_3$, DIEA, 84%; (iii) 2,2-dimethoxyethanamine; (iv) HCl, 59% (2 steps); (v) mCPBA, 92%; (vi) amine.

treated with NaH and a halo-substituted isocyanatobenzene to afford the bicyclic intermediate **5**.[16] The pyrimidinedione moiety was chlorinated in the presence of $POCl_3$ and DIEA. An S_NAr addition using 2,2-dimethoxyethanamine led to **7**, which was subsequently cyclized under acid conditions. The methyl thioether group of **8** was oxidized by mCPBA, setting the stage for the final S_NAr reaction with a desired amino substrate to provide **10**–**25**.[17] Compounds **26** to **31** were synthesized in the same fashion using the corresponding bis-halo isocyanatobenzene in the first step.

The binding affinity of all compounds, presented as K_i values, was assessed in a routine 6-point TR-FRET binding assay. A functional antiproliferative cell viability assay and a mechanism-based pCDK1 ELISA assay, both utilizing the NCI-H1299 cell line (human nonsmall cell lung carcinoma) to provide EC_{50} values, helped to access cellular potency of any potent binders. It was gratifying to find that the first analogue synthesized, **10**, was active in the biochemical assay (K_i = 2.3 nM) and also possessed reasonable cellular activity in both the cell viability and ELISA assays (EC_{50} = 1.0 and 0.37 μM, respectively). According to the model of compound **10** bound to the Wee1 active site (Figure 1A), one of the pyrimidine nitrogens and the tethered amino group form hydrogen-bond interactions to the backbone NH and backbone carbonyl O of residue Cys379, respectively (i.e., a two-hinge interaction motif). The model also predicted a third, nonhinge, H-bond interaction between the side-chain N of Wee1 gatekeeper residue Asn376 and the amide carbonyl O in compound **10**. This third H-bond interaction was believed to be critical for good kinase

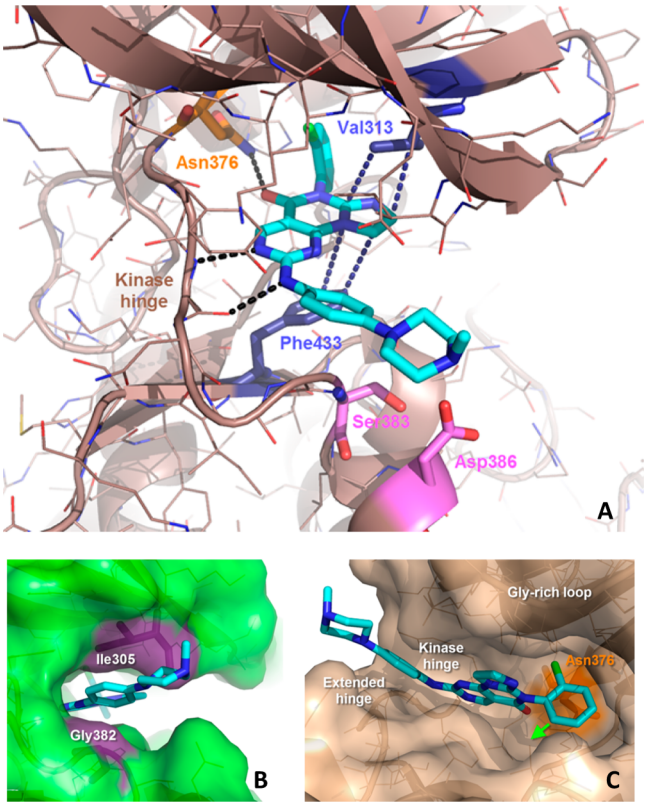

Figure 1. (A) Computational molecular model of compound **10** (shown in cyan, stick) bound to the Wee1 kinase binding site (shown in brown, ribbon). Key residues are shown in stick. The ligand is predicted to make three H-bond interactions with the protein (black dashes). Two of these interactions are made with backbone polar atoms in the hinge. The third interaction is made with the side chain of gatekeeper residue Asn376 (shown in orange, stick). The 5-membered ring added to the original bicyclic core (leading to the novel tricyclic core) is predicted to be sitting in a sweet spot right between Phe433 located at the base of the ATP binding site, and Val313 located in the Gly-rich loop. Purple dashes indicate the extent of the "sandwich" made by these two residues. (B) Close fit of benzene ring (part of R group) with surrounding protein walls, defined by residues Ile305 (Gly-rich loop) and Gly382 (extended hinge). (C) Halogenated phenyl ring uses small pocket next to gatekeeper residue Asn376 (shown in orange), while sitting perpendicular to tricyclic core. Green arrow indicates unutilized space.

selectivity[18] since human kinases rarely have a hydrogen-bond donor (HBD) residue such as Asn in the gatekeeper position (<0.5% of ~500 human kinases based on internal studies).

Encouraged by these early results, we proceeded to map the structure–activity relationship (SAR) of the aminoaryl group attached to the pyrimidine ring. Removing the terminal piperazine on **10** led to about 10-fold loss in potency (**11**), while the importance of the aminoaryl moiety is clearly demonstrated with **12** being inactive (K_i >3140 nM) (Table 1). The reason for loss of activity by replacing the benzene with cyclohexane is likely due to the nature of the "gate" region leading to the ATP binding site (Figure 1B). Aromatic rings such as benzene are the ideal fit for this region in the protein, i.e., they are properly "sandwiched" between residue Gly382 (located in the extended hinge region) and residue Ile305 (located in the Gly-rich loop). Pi–sigma interactions between the aromatic ring in the ligand and aliphatic C–H bonds in the protein (alpha-C of Gly382 and beta-C of Ile305) are the main drivers behind the optimal

Table 1. Mono-Cl Analogues

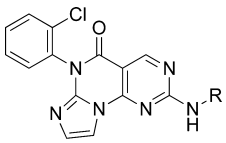

ID	R	Ki (nM)	H1299 EC_{50} (μM)[a]	pCDK1 EC_{50} (μM)[b]
10	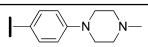	2.3	1.0	0.37
11		21	5.9	6.8
12		>3140	N.T.	N.T.
13	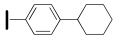	87	>10	>10
14	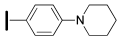	5.5	9.8	3.8
15	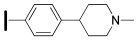	8.3	9.6	3.1
16	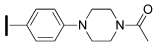	6.6	3.3	1.1
17	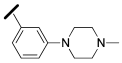	6.2	6.5	1.5
18	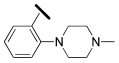	>3140	N.T.	N.T.
19		26	7.3	6.0
20	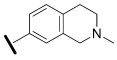	1.6	0.77	0.22
21		8.6	>10	2.3
22		7.4	9.3	2.7
23	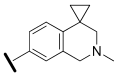	1.2	0.69	0.10
24	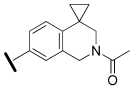	5.4	2.0	0.62
25	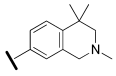	<1.0	0.55	0.098

[a]Cell viability assay. [b]ELISA assay in H1299 cells. All data were an average of at least two measurements except for those with a qualifier or high micromolar values. N.T.: not tested.

protein–ligand complementarity observed in this region. Unlike benzene, saturated rings such as cyclohexane are too voluminous to fit well in this somewhat narrow region of the kinase binding site. At least one nitrogen atom of the piperazine on **10** was needed to maintain a K_i value below 10 nM (**13**–**15**), although reducing the basicity of the terminal nitrogen through acylation had little impact on Wee1 binding (**16**). Highly hydrophobic groups such as the cyclohexyl on **13** do not match well with the local environment in this solvent exposed region of the kinase, dominated by polar residues Ser383 (ribose residue) and Asp386 (ribose + 3 residue) shown in Figure 1A. Once the ligand tail starts to project into solvent, R groups with a larger polar surface area (PSA), such as those in **14**–**16**, are much better choices. Moving the piperazine to the meta position of the benzene maintained the potency (**17**, K_i = 6.2 nM); however, placing it at the ortho position was not tolerated (**18**). Piperazine at the meta position confers the ligand a global conformation that still matches the V-shape/C-shape needed to complement the kinase binding site. Unfortunately, piperazine at the ortho position locks the ligand in a new conformation that is no longer compatible with the shape of the target binding site. Next, we investigated the SAR of bicyclic scaffolds with a saturated ring fused to the benzene. Once again, the presence of a nitrogen atom on the saturated ring was desirable for enzymatic potency (**19** vs **20**–**22**). Among these analogues, the tetrahydroisoquinoline inhibitor, **20**, exhibited much better cellular activities and was the focus of further optimization. Installing a cyclopropyl group at the 4-position of the isoquinoline of **20** led to **23**, another analogue not only with high enzymatic potency (K_i =1.2 nM) but also possessing sub-micromolar activity in the cell viability (EC_{50} = 0.69 μM) and pCDK1 ELISA (EC_{50} = 0.10 μM) assays. Acylation of the tetrahydroisoquinoline nitrogen brought a slight deterioration in activity (**24**). The *gem*-dimethyl analogue, **25**, showed overall potent activity comparable to **23**. Four representative compounds (**10**, **20**, **23**, and **25**) were evaluated for their pharmacokinetic (PK) profile in mice (Table 2). Even though they all demonstrated desirable profiles, **25** appeared to have the best overall properties. The *iv* half-life reached 2.8 h, while clearance was modest (1.4 L/h/kg) with oral biovailability of 80%.

Table 2. Mouse PK for Mono-Cl Analogues[a]

ID	*iv* $t_{1/2}$ (h)	*iv* CL (L/h/kg)	*po* AUC (μM·h)	*po* F (%)
10	1.9	1.8	8.4	72
20	1.5	2.2	5.2	52
23	2.3	1.5	9.8	70
25	2.8	1.4	12.3	80

[a]CD-1 mouse. *iv* dosing: 3 mg/kg. *po* dosing: 10 mg/kg.

Having gained much insight in the SAR of the aminoaryl region, we turned our attention to the modification of the chloro-benzene ring (Table 3). Modeling suggested that the *ortho*-Cl group is essential for situating the phenyl moiety *orthogonal* to the tricyclic core (Figure 1C). Not only is the intramolecular arrangement optimal when the phenyl group is rotated almost 90° with respect to the plane of the tricyclic core, but the space available in the pocket (adjacent to gatekeeper residue Asn376) is also limited, and it can only accommodate such a large ring if placed "facing" the gatekeeper residue. The benefit of adding an extra halo substitution at the other ortho position is 2-fold. On one hand, the 2,6-disubstitution pattern reinforces the 90° rotation needed for optimal complementarity with the immediate surroundings. On the other hand, the second halogen fills the remaining portion of the pocket (otherwise empty, i.e., with only a monosubstituted phenyl), increasing van der Waals contacts with the protein, and further increasing compound affinity/potency. Not surprisingly, all bis-halo analogues (**26** to **31**) demonstrated potent activity in the biochemical assay with K_i values below the lower detection limit for all except **27**. The potent binding affinity was presumably responsible for the generally superior cellular activities possessed by this group of compounds. Four

Table 3. Bis-Halo Analogues

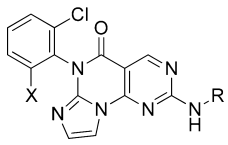

ID	R	X	Ki (nM)	H1299 EC_{50} (μM)[a]	pCDK1 EC_{50} (μM)[a]
26	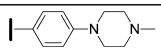	Cl	<1.0	0.19	0.087
27	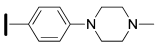	F	2.0	0.45	0.17
28	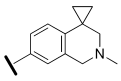	Cl	<1.0	0.22	0.027
29	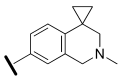	F	<1.0	0.21	0.029
30	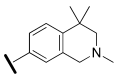	Cl	<1.0	0.23	<0.013[b]
31	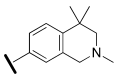	F	<1.0	0.31	0.060

[a]Average of two measurements. [b]Values of 0.013 and <0.010 μM.

compounds (**26** and **29**–**31**) were chosen for mouse PK studies with comparably favorable properties to that observed for the mono-Cl compounds (Table 4). The best compound, **31**, achieved an adequate *iv* half-life (2.8 h), low clearance (0.55 L/h/kg), and excellent oral biovailability (F = 94%).

Table 4. Mouse PK for Bis-Halo Analogues[a]

ID	*iv* $t_{1/2}$ (h)	*iv* CL (L/h/kg)	*po* AUC (μM·h)	*po* F (%)
26	1.7	2.0	6.5	55
29	2.6	1.1	12	68
30	3.9	0.97	9.8	49
31	2.8	0.55	24	94

[a]CD-1 mouse. *iv* dosing: 3 mg/kg. *po* dosing: 10 mg/kg.

Compound **31** was dosed orally at 100 mg/kg/day (mkd) in H1299 tumor bearing mice (n = 4), utilizing inhibition of pY15 Cdk1/2 as an *in vivo* pharmacodynamics marker of Wee1 inhibition. The resulting Western immunoblotting analysis (Figure 2) demonstrated a nearly complete depletion of the pY15 bands at both 6 and 10 h after dosing. The concentration of **31** in plasma decreased 32% between these two time points, however, the tumor exposure levels remained at high throughout (47 and 53 μM).

Compound **31** was further evaluated for its activity in potentiating the efficacy of the cytotoxic agent, irinotecan, in a mouse xenograft model (H1299). As presented in Chart 1, **31** achieved a modest tumor growth inhibition (TGI) of 43% (p < 0.001) after oral dosing at 50 mkd on day 41. Meanwhile, irinotecan alone reached a TGI of 67% (p < 0.001) at 10 mkd. The combination of **31** and irinotecan achieved an 83% TGI (p < 0.001). On day 52, the combination group showed a 58% TGI when compared to irinotecan alone (p < 0.05). The durability of the combination response was highlighted by a 25% tumor growth delay (TGD) when compared to irinotecan alone (p < 0.01). All dosing regimens were well tolerated. Furthermore, the efficacy of **31** to sensitize irinotecan appeared to be dose responsive.[19] Together, these results highlight the combination efficacy of **31** with irinotecan *in vivo*.

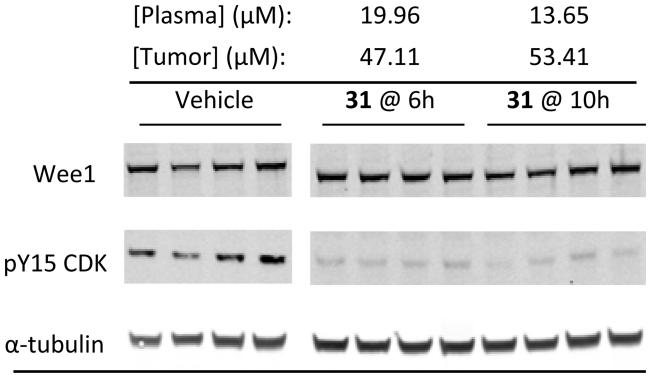

Figure 2. Pharmacodynamic profiles of compound **31**. Biomarker effects of **31** on expression of pY15 in H1299 tumor bearing mice after *po* dosing (100 mkd) as analyzed by Western blot. Loading control: α-tubulin.

Chart 1. Tumor Growth Inhibition[a]

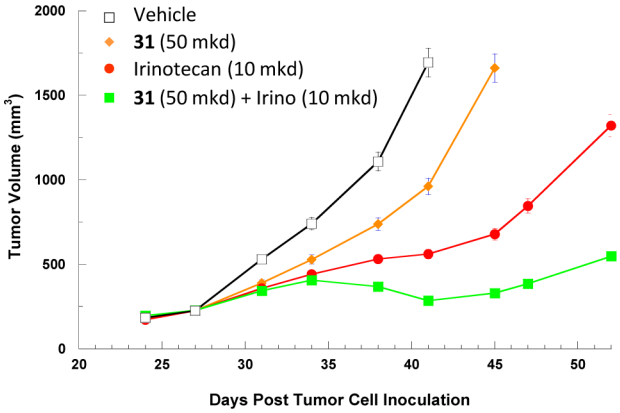

[a]Mouse xenograft (H1299 cell) data with tumor volume 52 days post-tumor inoculation. Compound **31** was orally dosed QD ×14 from day 28 to day 41. Irinotecan was dosed IP at days 28, 32, 36, and 40.

As disclosed in this letter, compounds with a pyrimidine-based tricyclic core were suggested by design/modeling and supported by their binding and cellular activity as potent Wee1 inhibitors. These molecules are generally selective against other kinases.[18] SAR studies in the aminoaryl and halo-benzene regions led to compounds with sub-nM K_i values in the enzymatic assay and sub-μM EC_{50} values in both functional and mechanism-based cell assays. Representative inhibitors also exhibited desirable pharmacokinetic profiles. Compound **31** demonstrated oral *in vivo* efficacy in a mouse H1299 xenograft model and potentiated the antiproliferative activity of irinotecan. These results suggest that this class of compounds may have potential as therapeutic agents for anticancer indications.

■ ASSOCIATED CONTENT

Supporting Information

Assay protocols, kinome selectivity profile, modeling protocols, efficacy study protocols, and synthetic procedures. This material is available free of charge via the Internet at http://pubs.acs.org.

dx.doi.org/10.1021/ml5002745 | ACS Med. Chem. Lett. 2015, 6, 58–62

AUTHOR INFORMATION

Corresponding Author

*(Y.T.) Phone: 1-847-935-1252. Fax: 1-847-935-5165. E-mail: yunsong.tong@abbvie.com.

Notes

The authors declare the following competing financial interest(s): All authors are employees of AbbVie. The design, study conduct, and financial support for this research were provided by AbbVie. AbbVie participated in the interpretation of data, review, and approval of the publication.

REFERENCES

(1) Ma, C. X.; Janetka, J. W.; Piwnica-Worms, H. Death by releasing the breaks: CHK1 inhibitors as cancer therapeutics. *Trends Mol. Med.* **2011**, *17*, 88−96.

(2) Do, K.; Doroshow, J. H.; Kummar, S. Wee1 kinase as a target for cancer therapy. *Cell Cycle* **2013**, *12*, 3159−3164.

(3) Parker, L. L.; Piwnica-Worms, H. Inactivation of the p34cdc2-cyclin B complex by the human WEE1 tyrosine kinase. *Science* **1992**, *257*, 1955−1957.

(4) Stumpff, J.; Duncan, T.; Homola, E.; Campbell, S. D.; Su, T. T. Drosophila Wee1 kinase regulates Cdk1 and mitotic entry during embryogenesis. *Curr. Biol.* **2004**, *14*, 2143−2148.

(5) Vriend, L. E. M.; De Witt Hamer, P. C.; Van Noorden, C. J. F.; Wüerdinger, T. WEE1 inhibition and genomic instability in cancer. *Biochim. Biophys. Acta* **2013**, *1836*, 227−235.

(6) Iorns, E.; Lord, C. J.; Grigoriadis, A.; McDonald, S.; Fenwick, K.; MacKay, A.; Mein, C. A.; Natrajan, R.; Savage, K.; Tamber, N.; Reis-Filho, J. S.; Turner, N. C.; Ashworth, A. Integrated functional, gene expression and genomic analysis for the identification of cancer targets. *PLoS One* **2009**, *4*, e5120.

(7) Mir, S. E.; De Witt Hamer, P. C.; Krawczyk, P. M.; Balaj, L.; Claes, A.; Niers, J. M.; Van Tilborg, A. A. G.; Zwinderman, A. H.; Geerts, D.; Kaspers, G. J. L.; Peter Vandertop, W.; Cloos, J.; Tannous, B. A.; Wesseling, P.; Aten, J. A.; Noske, D. P.; Van Noorden, C. J. F.; Wüerdinger, T. In silico analysis of kinase expression identifies wee1 as a gatekeeper against mitotic catastrophe in glioblastoma. *Cancer Cell* **2010**, *18*, 244−257.

(8) Magnussen, G. I.; Holm, R.; Emilsen, E.; Rosnes, A. K. R.; Slipicevic, A.; Floerenes, V. A. High expression of Wee1 is associated with poor disease-free survival in malignant melanoma: potential for targeted therapy. *PLoS One* **2012**, *7*, e38254.

(9) Mizuarai, S.; Yamanaka, K.; Itadani, H.; Arai, T.; Nishibata, T.; Hirai, H.; Kotani, H. Discovery of gene expression-based pharmacodynamic biomarker for a p53 context-specific anti-tumor drug Wee1 inhibitor. *Mol. Cancer* **2009**, *8*, 34.

(10) Palmer, B. D.; Thompson, A. M.; Booth, R. J.; Dobrusin, E. M.; Kraker, A. J.; Lee, H. H.; Lunney, E. A.; Mitchell, L. H.; Ortwine, D. F.; Smaill, J. B.; Swan, L. M.; Denny, W. A. 4-Phenylpyrrolo[3,4-c]carbazole-1,3(2*H*,6*H*)-dione inhibitors of the checkpoint kinase wee1. Structure−activity relationships for chromophore modification and phenyl ring substitution. *J. Med. Chem.* **2006**, *49*, 4896−4911.

(11) Palmer, B. D.; Smaill, J. B.; Rewcastle, G. W.; Dobrusin, E. M.; Kraker, A.; Moore, C. W.; Steinkampf, R. W.; Denny, W. A. Structure−activity relationships for 2-anilino-6-phenylpyrido[2,3-d]-pyrimidin-7(8*H*)-ones as inhibitors of the cellular checkpoint kinase Wee1. *Bioorg. Med. Chem. Lett.* **2005**, *15*, 1931−1935.

(12) For a recent review, see De Witt Hamer, P. C.; Mir, S. E.; Noske, D.; Van Noorden, C. J. F.; Wüerdinger, T. WEE1 kinase targeting combined with dna-damaging cancer therapy catalyzes mitotic catastrophe. *Clin. Cancer Res.* **2011**, *17*, 4200−4207.

(13) Bamba, M.; Furuyama, H.; Niiyama, K.; Sakamoto, T.; Sunami, S.; Takahashi, K.; Yamamoto, F.; Yoshizumi, T. Bicycloaniline derivative. WO 2008/15307, December 18, 2008.

(14) Squire, C. J.; Dickson, J. M.; Ivanovic, I.; Baker, E. N. Structure and inhibition of the human cell cycle checkpoint kinase, wee1a kinase: an atypical tyrosine kinase with a key role in CDK1 regulation. *Structure* **2005**, *13*, 541−550.

(15) Smaill, J. B.; Baker, E. N.; Booth, R. J.; Bridges, A. J.; Dickson, J. M.; Dobrusin, E. M.; Ivanovic, I.; Kraker, A. J.; Lee, H. H.; Lunney, E. A.; Ortwine, D. F.; Palmer, B. D.; Quin, J., III; Squire, C. J.; Thompson, A. M.; Denny, W. A. Synthesis and structure-activity relationships of N-6 substituted analogues of 9-hydroxy-4-phenylpyrrolo[3,4-c]carbazole-1,3(2*H*,6*H*)-diones as inhibitors of Wee1 and Chk1 checkpoint kinases. *Eur. J. Med. Chem.* **2008**, *43*, 1276−1296.

(16) Bamba, M.; Sunami, S. Dihydropyrimidopyrimidine derivatives. WO 2010/067888, June 17, 2010.

(17) Synthesis of **20** involved the addition of *tert*-butyl 7-amino-3,4-dihydroisoquinoline-2(1*H*)-carboxylate followed by Boc removal and methylation on the isoquinoline nitrogen. Synthesis of **24** involved the addition of *t*-butyl 7′-amino-1′*H*-spiro[cyclopropane-1,4′-isoquinoline]-2′(3′*H*)-carboxylate followed by Boc removal and acylation on the isoquinoline nitrogen. See Supporting Information for detailed procedures.

(18) Kinome profiling of a few key inhibitors against 84 kinases is provided in the Supporting Information.

(19) Efficacy of **31** at a higher dose and more detailed biology studies will be published elsewhere.